

# Structural isomers of the $S_2$ state in photosystem II: do they exist at room temperature and are they important for function?

Ruchira Chatterjee<sup>a</sup> , Louise Lassalle<sup>a</sup>, Sheraz Gul<sup>a</sup> , Franklin D. Fuller<sup>a</sup>, Iris D. Young<sup>a</sup>, Mohamed Ibrahim<sup>b</sup>, Casper de Lichtenberg<sup>c,d</sup>, Mun Hon Cheah<sup>c</sup>, Athina Zouni<sup>b</sup>, Johannes Messinger<sup>c,d,\*</sup> , Vittal K. Yachandra<sup>a,\*</sup>, Jan Kern<sup>a,\*</sup>  and Junko Yano<sup>a,\*</sup> 

<sup>a</sup>Molecular Biophysics and Integrated Bioimaging Division, Lawrence Berkeley National Laboratory, Berkeley, CA 94720, USA

<sup>b</sup>Institut für Biologie, Humboldt-Universität zu Berlin, Berlin D-10099, Germany

<sup>c</sup>Department of Chemistry – Ångström, Molecular Biomimetics, Uppsala University, Uppsala 75237, Sweden

<sup>d</sup>Institutionen för Kemi, Kemiskt Biologiskt Centrum, Umeå Universitet, Umeå 90187, Sweden

## Correspondence

\*Corresponding authors,  
e-mail: johannes.messinger@kemi.uu.se;  
vkyachandra@lbl.gov; jfkern@lbl.gov;  
jyano@lbl.gov

Received 7 December 2018;  
revised 16 February 2019

doi:10.1111/ppl.12947

In nature, an oxo-bridged  $Mn_4CaO_5$  cluster embedded in photosystem II (PSII), a membrane-bound multi-subunit pigment protein complex, catalyzes the water oxidation reaction that is driven by light-induced charge separations in the reaction center of PSII. The  $Mn_4CaO_5$  cluster accumulates four oxidizing equivalents to enable the four-electron four-proton catalysis of two water molecules to one dioxygen molecule and cycles through five intermediate S-states,  $S_0 - S_4$  in the Kok cycle. One important question related to the catalytic mechanism of the oxygen-evolving complex (OEC) that remains is, whether structural isomers are present in some of the intermediate S-states and if such equilibria are essential for the mechanism of the O-O bond formation. Here we compare results from electron paramagnetic resonance (EPR) and X-ray absorption spectroscopy (XAS) obtained at cryogenic temperatures for the  $S_2$  state of PSII with structural data collected of the  $S_1$ ,  $S_2$  and  $S_3$  states by serial crystallography at neutral pH (~6.5) using an X-ray free electron laser at room temperature. While the cryogenic data show the presence of at least two structural forms of the  $S_2$  state, the room temperature crystallography data can be well-described by just one  $S_2$  structure. We discuss the deviating results and outline experimental strategies for clarifying this mechanistically important question.

## Introduction

In oxygenic photosynthesis, light-driven water oxidation to molecular oxygen is carried out by the oxygen-evolving complex (OEC) in photosystem II (PSII), which is a multisubunit protein complex in the thylakoid membrane of plants, algae and cyanobacteria

(Wydrzynski and Satoh 2005, Renger 2008). The OEC consists of four oxo-bridged Mn atoms and one Ca atom ( $Mn_4CaO_5$ ) ligated to the D1 protein and chlorophyll-protein CP43 subunits by carboxylate and histidine ligands (Umena et al. 2011). During water oxidation, the  $Mn_4CaO_5$  complex cycles through five intermediate states, collectively called the S-states,

*Abbreviations* – DFT, density functional theory; EPR, electron paramagnetic resonance; EXAFS, extended X-ray absorption fine structure; MLS, multiline signal; NIR, near-infrared; OEC, oxygen-evolving complex; PSII, photosystem II; RIXS, resonant inelastic X-ray spectroscopy; SR, synchrotron radiation; XES, X-ray emission spectra; XFEL, X-ray free electron laser.

labeled S<sub>0</sub>–S<sub>4</sub> in the Kok cycle (Kok et al. 1970). S<sub>0</sub> is the most reduced state, while S<sub>1</sub>, S<sub>2</sub> and S<sub>3</sub> represent sequentially higher oxidation states in the OEC. O<sub>2</sub> is released during the S<sub>3</sub> → [S<sub>4</sub>] → S<sub>0</sub> transition, where S<sub>4</sub> is a transient state. Thus, the Mn<sub>4</sub>CaO<sub>5</sub> cluster accumulates four oxidizing equivalents before the release of O<sub>2</sub>. The formal oxidation state of each S-state has been assigned as Mn<sub>4</sub><sup>III,III,III,IV</sup> for S<sub>0</sub>, Mn<sub>4</sub><sup>III,III,IV,IV</sup> for S<sub>1</sub>, Mn<sub>4</sub><sup>III,IV,IV,IV</sup> for S<sub>2</sub> and Mn<sub>4</sub><sup>IV,IV,IV,IV</sup> for S<sub>3</sub> (Haumann et al. 2005, Dau and Haumann 2008, Yano and Yachandra 2014). Increased delocalization of the charge in the Mn complex has also been proposed, especially, in the higher S-states, using data from resonant inelastic X-ray spectroscopy (RIXS) experiments (Glatzel et al. 2004, 2013).

Recently, we reported the structures of the catalytic intermediate states of PSII in the dark (0F; S<sub>1</sub>-rich), 1F (S<sub>2</sub>-rich), 2F (S<sub>3</sub>-rich) and 3F (S<sub>0</sub>-rich) states with resolutions of 2.04–2.08 Å (Kern et al. 2018). Data were collected at an X-ray Free Electron Laser (XFEL) with femtosecond X-ray pulses at room temperature (RT), by *in situ* visible light excitation to advance the S-states. Improved resolution approaching 2 Å unambiguously reveals oxygen and metal atomic positions in the catalytic center in each state. K $\beta_{1,3}$  X-ray emission spectra (XES) were simultaneously collected from crystals to provide confirmation of catalytic advancement by probing the changes in the oxidation state of the metal cluster (Kern et al. 2013, 2014, 2018, Fuller et al. 2017, Fransson et al. 2018), together with the oxidation state changes of the mobile quinone Q<sub>B</sub> site, evidenced by its electron density changes. Availability of the structural data for each stable intermediate state now enables us to reexamine previous X-ray spectroscopy data based on the new structural information.

One of the important questions regarding the OEC is the presence or absence of structural isomers in each S-state and its catalytic role (Pantazis et al. 2012, Renger 2012, Cox et al. 2014, Isobe et al. 2014). Spin isomers indeed exist, as shown by the various EPR studies in the S<sub>2</sub> state [reviewed in (Haddy 2007, Pokhrel and Brudvig 2014)]. Yet, whether such isomers play an important role in the catalytic mechanism has not been shown experimentally. For example, the importance of the spin isomorphism observed in the S<sub>2</sub> state has been suggested in recent studies (Pantazis et al. 2012, Cox et al. 2014, Isobe et al. 2014), in relation to the formation of the S<sub>3</sub> state, where the chemical environment is prepared for the O-O bond formation to occur in the following steps. Similarly, there have been suggestions of isomorphism in the S<sub>1</sub> (S<sub>total</sub>=0 and S<sub>total</sub>=1) and S<sub>3</sub> states (S<sub>total</sub>=3 and an undetermined higher spin state that is not detected by EPR), all of which are detected under

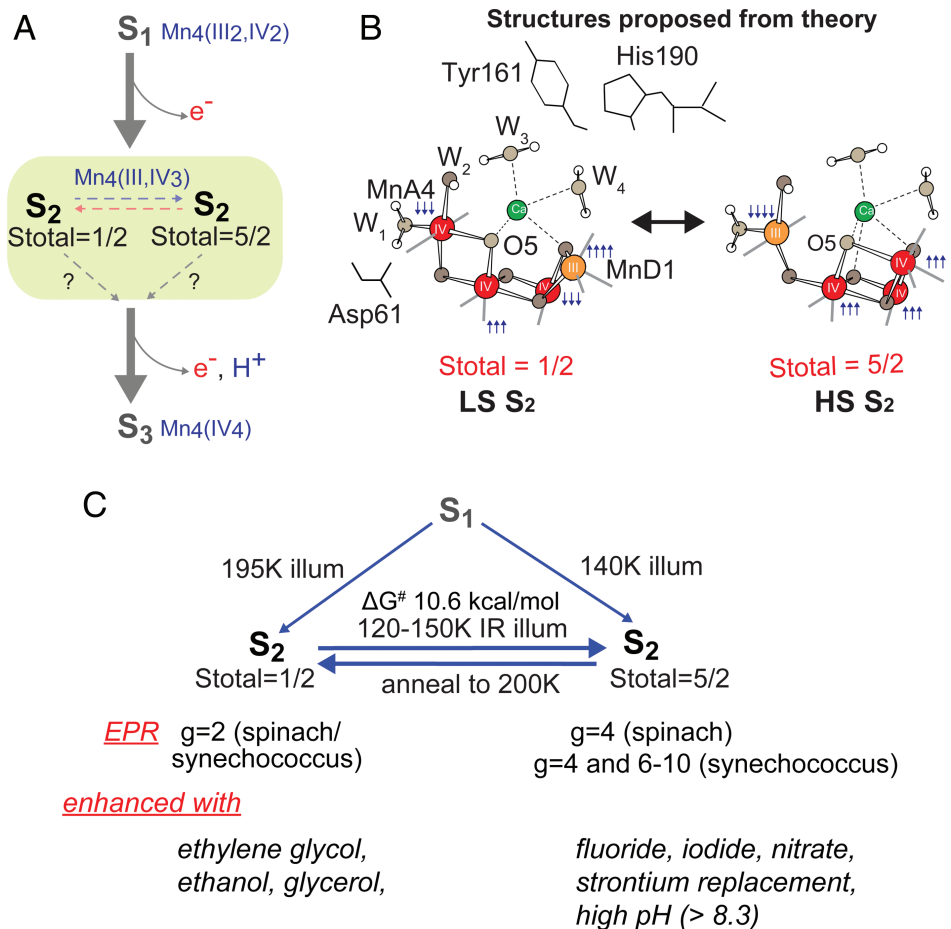
cryogenic temperatures (Boussac et al. 2009, Cox et al. 2014, Isobe et al. 2014, 2016, Lubitz et al. 2014, Shoji et al. 2018). The presence and population of the isomers in each S-state under physiological conditions remains to be established. The difficulty to prove the role of isomers, also stems from the fact that each set of experimental data contains its own uncertainty and they are often collected under different experimental conditions. Thus, understanding if the structural and electronic heterogeneity is functionally important or caused due to variations in experimental conditions becomes important.

In this review, we focus on the S<sub>2</sub> state by examining the room temperature S<sub>2</sub> state crystal structure and comparing it with the previous results from EPR and synchrotron X-ray spectroscopy at cryogenic temperature. In the S<sub>2</sub> state, EPR studies by several groups (Krewald et al. 2016, reviewed in Haddy 2007, Pokhrel and Brudvig 2014) suggest the presence of isomorphous structures within the same redox/intermediate S-state, i.e. S<sub>2</sub> with a high-spin (HS, S<sub>total</sub>=5/2) and a low spin (LS, S<sub>total</sub>=1/2) form (Fig. 1A,B). As discussed above, it has been proposed that such geometric and electronic structural flexibility in S<sub>2</sub> may play a role in the formation of the S<sub>3</sub> state through water binding (Pantazis et al. 2012, Cox et al. 2013, Cox and Messinger 2013, Isobe et al. 2014, Ugur et al. 2016, Boussac et al. 2018). Our XAS studies using synchrotron radiation (SR) at cryogenic temperature also shows differences in the geometric and electronic structure of the cryo-trapped HS and LS S<sub>2</sub> states (Chatterjee et al. 2016). Such structural and magnetic redox-isomers, if present at RT, will probably play a role during the catalysis for determining the directionality and the kinetics of the reaction. The room temperature crystallography study provides a tool to visualize the role of such structural heterogeneity. We show that, under our experimental conditions of crystallography at neutral pH (~6.5), the dominant form in the S<sub>2</sub> state is the right-open structure with a low spin configuration that geometrically resembles the dark stable S<sub>1</sub> state structure. However, differences are observed in the atomic distances and positions of surrounding waters between the S<sub>1</sub> and the S<sub>2</sub> states.

## Background

Among the S-states, the S<sub>2</sub> state is the most studied state because of the presence of rich EPR signals and nearly 100% conversion by illumination starting from the dark stable S<sub>1</sub> state. The subsequent S<sub>2</sub> to S<sub>3</sub> state transition is accompanied by noticeable Mn-Mn distance changes (Guiles et al. 1990, Liang et al. 1994, Pushkar et al. 2008, Glöckner et al. 2013), and several factors such as Ca-depletion, site-specific mutations and chemical

**Fig. 1.**  $S_2$ -g2 and  $S_2$ -g4 transition. (A) Transition scheme from  $S_1$  to the  $S_2$ -g2 and  $S_2$ -g4 states in PSII from plants and the oxidation states of the Mn and the total spin of  $S$ -states. (B) Proposed HS and LS  $S_2$  state structures by Pantazis et al. 2012 and Isobe et al. 2014. (C) Formation and the conversion between the  $S_2$ -g2 and  $S_2$ -g4 state and the difference in their physical properties. A detailed discussion can be found in several reviews and papers (Haddy 2007, Pokhrel and Brudvig 2014, Boussac et al. 2015, 2018).



treatments (e.g. with fluoride) are known to block this advance (Debus 1992, Haddy 2007, Pokhrel and Brudvig 2014, Boussac et al. 2015). The requirement for a structural change, and its susceptibility to many chemical and biochemical treatments, makes the  $S_2$  to  $S_3$  transition one of the critical steps for the water oxidation reaction during the  $S$ -state cycle.

In the  $S_2$  state, two types of EPR signals have been assigned to the Mn cluster (Figs 1 and 2A). The multiline signal (MLS) centered at  $g=2$ , exhibiting at least 18 partially resolved hyperfine lines at X-band ( $\sim 9$  GHz), is assigned to a low spin ( $S_{\text{total}} = 1/2$ , i.e. Mn<sup>III</sup>/Mn<sup>IV</sup> and Mn<sup>IV</sup>/Mn<sup>IV</sup> are anti-ferromagnetically coupled, respectively) ground state, LS  $S_2$  state (Dismukes and Siderer 1981, Hansson and Andréasson 1982, Brudvig et al. 1983, de Paula and Brudvig 1985, Randall et al. 1995, Peloquin et al. 2000, Charlot et al. 2005, Haddy 2007, Kulik et al. 2007, Cox et al. 2011). Another broad featureless EPR signal at  $g \geq 4.1$ , attributed to a higher spin multiplicity ( $S_{\text{total}} = 5/2$ , i.e. ferromagnetically coupled three Mn<sup>IV</sup> with anti-ferromagnetically coupled one Mn<sup>III</sup>) ground state, HS  $S_2$  state, is also observed under

different experimental conditions (Casey and Sauer 1984, Zimmermann and Rutherford 1984, Boussac et al. 1996, 1998a,b, Peloquin and Britt 2001, Haddy et al. 2004).

The high ( $S_{\text{total}} = 5/2$ ) and low spin ( $S_{\text{total}} = 1/2$ ) forms in the  $S_2$  state are interrelated, on the basis of the observation of the amplitude conversion of the  $S_2$ -g4 EPR signal to the  $S_2$ -g2 EPR signal (Casey and Sauer 1984, Beck and Brudvig 1986, Zimmermann and Rutherford 1986, Hansson et al. 1987). The distribution of high spin and low spin species and the  $g$ -values and hyperfine coupling values of these spin states are sensitive to several parameters, such as (a) species (higher-plant, thermophile or non-thermophile cyanobacterial PSII) in different pHs, (b) the presence of chemical additives such as alcohol (methanol or ethanol) or sucrose and glycerol (often used as cryo-protectant) in the sample, (c) substitution of the native Ca<sup>2+</sup> in the OEC (Ca<sup>2+</sup>-PSII) by Sr (Sr<sup>2+</sup>-PSII) and (d) halide substitution in PSII with Br<sup>-</sup> or I<sup>-</sup> replacing the Cl<sup>-</sup> of the native state (Fig. 1C). A detailed discussion can be found in several reviews (Haddy 2007, Pokhrel and Brudvig 2014, Boussac et al. 2015, 2018).

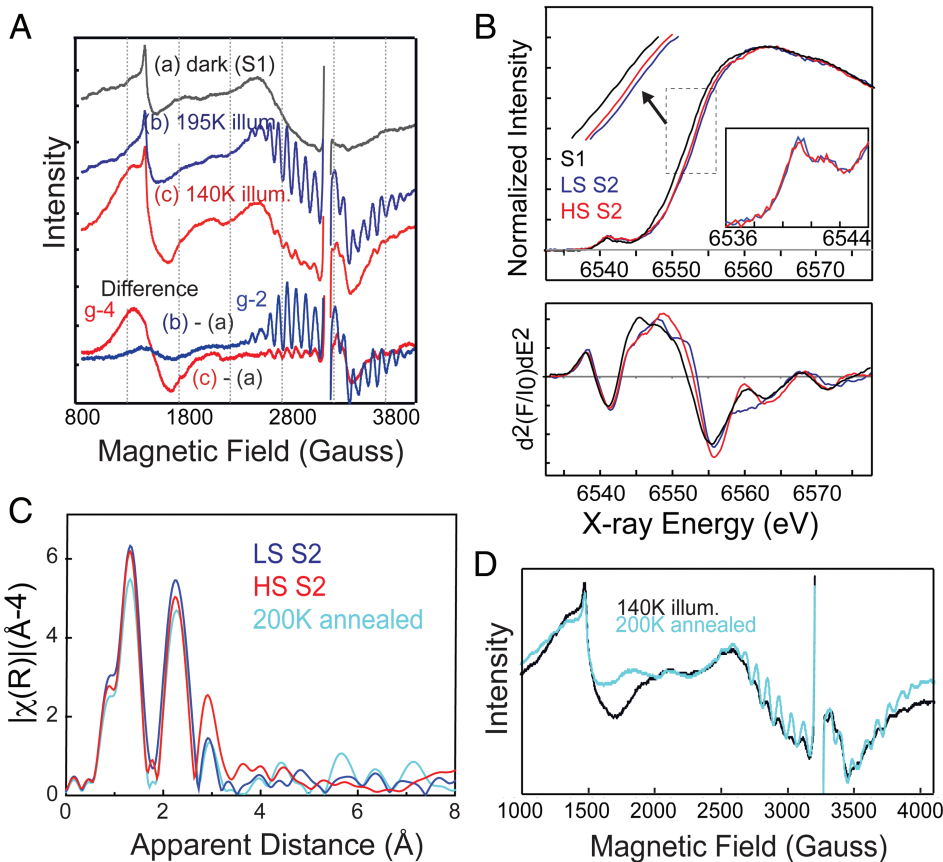


**Fig. 2.** EPR and XAS spectra of spinach PSII. (A) EPR spectra of spinach PSII samples illuminated at 195 K (blue) and 140 K with NIR (red) along with corresponding dark (black) EPR spectra. The difference spectra are between the spectra after illumination and the spectra of the same dark-adapted sample. (B) Mn XANES spectra (top) and their second derivative spectra (bottom) of HS (red) and LS (blue)  $S_2$  states, in comparison with  $S_1$  (black) states. (C) Mn EXAFS spectra of HS (red) and LS (blue)  $S_2$  states. The spectrum of the 140 K illuminated sample (HS-rich) after 200 K annealing is also shown (cyan). (D) EPR spectrum of the sample annealed at 200 K (cyan) after 140 K with illumination compared to the 140 K with NIR (black) spectrum. The figure is adapted from Chatterjee et al. 2016.

Briefly, in spinach PSII samples illuminated at 200 K, both  $S_2$ -g2 and  $S_2$ -g4 signals are observed in the presence of sucrose, while with glycerol, ethylene glycerol, or ethanol, the MLS is enhanced and the  $S_2$ -g4 EPR signal is suppressed (Zimmermann and Rutherford 1986). Some treatments such as (c) and (d) instead stabilize the  $S_{\text{total}} = 5/2$  state. Illumination by near-infrared (NIR) light at low temperature ( $\sim 150$  K) has been shown to convert the  $S_{\text{total}} = 1/2$  form to the  $S_{\text{total}} = 5/2$  form without further advancement of the S-state of the OEC (Zimmermann and Rutherford 1986, Boussac et al. 1998b). Subsequent annealing in the dark converts the  $S_{\text{total}} = 5/2$  form back to the  $S_{\text{total}} = 1/2$  form (Casey and Sauer 1984), showing that these two forms are interconvertible. PSII samples treated with  $F^-$ ,  $NO_3^-$  or  $I^-$  or when  $Ca^{2+}$  is replaced by  $Sr^{2+}$  have been reported to show an enhanced  $S_2$ -g4 signal with the line widths and g values being slightly different (Boussac and Rutherford 1988). In cyanobacterial PSII wild-type, along with the  $S_2$ -g4 signal additional EPR signals at  $g = 6$  to 10 are also observed when samples are illuminated with IR light. The pure  $g = 4$  signal is only observed when the native  $Ca^{2+}$  or  $Cl^-$  is substituted (Boussac et al. 2015). In this species, the intensity of these low EPR field signals are weak, suggesting that

the  $S_2$ -g2 state is the primary feature in the wild-type. The reason for such species dependence is not known, as the crystal structure is only available for PSII from the thermophilic cyanobacteria *Synechococcus elongatus* or *Synechococcus vulcanus*. However, it is probably due to small differences in the hydrogen-bonding network in the water channels surrounding the OEC that could lead to subtle differences in the electronic structure.

Recently, density functional theory (DFT) calculations suggested theoretical structural models corresponding to the two spin states (Pantazis et al. 2012, Bovi et al. 2013, Isobe et al. 2014, Narzi et al. 2014) and concluded that the two spin states, LS  $S_2$  and HS  $S_2$ , are almost isoenergetic. Ab initio molecular dynamics simulations by Bovi et al. (2013) showed that they can interconvert over a low barrier ( $\Delta G^\#$  of 10.6 kcal mol $^{-1}$ ). In the proposed models by Pantazis et al. (2012), the two spin states arise from a different location of  $Mn^{III}$ ; for  $g = 2$ ,  $Mn^{III}$  is located in the corner of the cubane motif ( $Mn_{D1}$ ), while for  $g > 4$ , it is located at the tail  $Mn_{A4}$  (Fig. 1B). In this study, the two spin isomers differ structurally, where LS  $S_2$  is ‘open’ (also called ‘right open structure’) with all four Mn connected in di- $\mu$ -oxo Mn-Mn interactions while HS  $S_2$  is a ‘closed’ structure with three Mn connected via di- $\mu$ -oxo

interactions and one Mn having a mono- $\mu$ -oxo interaction, this structure is also referred to as a closed ‘cubane’ with a ‘dangling Mn’ or as the ‘left open structure’. It has been suggested that such isomorphism makes O5 unique, and that O5 could become a likely candidate for the slow-exchanging water in the  $S_2$  state (Pantazis et al. 2012, Cox et al. 2013, Cox and Messinger 2013). It was further proposed that the structural change from LS  $S_2$  to HS  $S_2$  is a required (Narzi et al. 2014, Retegan et al. 2014) or favored (Ugur et al. 2016) intermediate step in the  $S_2$  to  $S_3$  transition.

EPR (Cox et al. 2013, 2014, Lubitz et al. 2014) and theoretical studies (Bovi et al. 2013, Siegbahn 2013, Narzi et al. 2014, Isobe et al. 2015, Shoji et al. 2015, Retegan et al. 2016, Ugur et al. 2016) proposed that there is an insertion of a water molecule in the  $Mn_4CaO_5$  cluster during the  $S_2$  to  $S_3$  transition. As the quality of the room temperature crystallography data of the  $S_3$  state has been improved compared to previous studies (Young et al. 2016, Suga et al. 2017), the exact position of the inserted water molecule is becoming clear, although its protonation state is still uncertain (Kern et al. 2018). It has been suggested from theory that this water insertion into the  $Mn_4CaO_5$  cluster is coupled with the interconversion of the two spin isomers, ‘open’ LS  $S_2$  and ‘closed’ HS  $S_2$  cubane, of the  $S_2$  state (Fig. 1B) as part of the  $S_2$  to  $S_3$  transition. These suggested models, largely based on theoretical calculations, can be summarized as follows: (1) for a terminal water-derived ligand to fill the open coordination site on MnD1, a chemical change, such as deprotonation of a water molecule, occurs during the interconversion of the two spin isomers, ‘open’ LS  $S_2$  and ‘closed’ HS  $S_2$ . It is suggested that the oxidation and formation of the Tyr<sub>Z</sub> radical in the LS  $S_2$  state reorients the dipole moment from the cationic imidazolium of His190 to Asp61 making this region of the OEC the locus of the negative charge, regardless of the formal oxidation state of MnA4 (Retegan et al. 2014). This is proposed to trigger proton transfer from one of the waters (W1) on MnA4 to Asp61, shifting the  $LS\ S_2 \leftrightarrow HS\ S_2$  equilibrium in favor of the high spin configuration. In this model, only the HS  $S_2$  state would be able to progress to the  $S_3$  state, and thus LS  $S_2$  needs to convert to HS  $S_2$  in order to advance (Narzi et al. 2014, Retegan et al. 2014, Yamaguchi et al. 2017). (2) Another suggestion is that the formation of the Tyr<sub>Z</sub> radical affects the pKa of W3 triggering its movement toward either MnA4 or MnD1 depending on whether the cubane is in the closed (HS) or open (LS) configuration (Debus 2008, Noguchi 2008, Ugur et al. 2016). The authors propose a spontaneous movement of W3 ( $OH^-$ ) in both spin states for closed cubane structures but only in the high spin state in the open cubane form (Ugur et al. 2016). The interconversion between LS  $S_2$

and HS  $S_2$  state is proposed to be kinetically feasible due to the calculated small energy gap of 0.3–1.2 kcal mol<sup>-1</sup> between the spin/conformational states. This suggests that the OEC might switch between the two conformations (open → closed) and/or spin states (low spin → high spin) in order to proceed to the  $S_3$  state. However, there is no experimental evidence confirming these predicted pathways so far. Therefore, taking snapshots during each S-state transition under physiological temperatures becomes a valuable approach, as described in the later section.

The  $S_2$  to  $S_3$  transition involves proton and electron transfers (Dau and Haumann 2008, Klauss et al. 2012, 2015, Cox and Messinger 2013). The proton release is proposed to take place before electron transfer to remove the excess positive charge in the  $S_2$  state, thereby reducing the redox potential of the OEC (Klauss et al. 2012, 2015, Noguchi 2015). It is also important to understand the role of Ca, as Ca depletion blocks the  $S_2$  to  $S_3$  transition (Debus 1992). This indicates that the hydrogen-bond network of water molecules near Ca may play an important role in the release of a proton and water insertion (Isobe et al. 2015, Shoji et al. 2015, Nakamura et al. 2016, Kim et al. 2018). Therefore, to understand the changes taking place in the  $S_2$  to  $S_3$  transition that involves electron, proton and water transfers, it is important to probe the structural changes of the water network occurring during the  $S_2$  to  $S_3$  transition. This is key toward understanding the mechanism of water oxidation.

### Cryo-trapped HS and LS $S_2$ states from spinach studied using Mn X-ray absorption spectroscopy

We have investigated the isomorphism in the  $S_2$  state using Mn K-edge X-ray absorption spectroscopy combined with supporting EPR characterization (Chatterjee et al. 2016). Fig. 2 shows the EPR and XAS spectra of the HS ( $g=4$ ) and LS ( $g=2$ )  $S_2$  state species from spinach PSII preparations. The two spin isomers of the  $S_2$  state in the spinach PSII samples were prepared by illumination at 140 or 195 K. The 195 K illumination for the LS ( $g=2$ )  $S_2$  state was performed in a dry ice/ethanol bath and samples were illuminated for 10 min using a 400 W tungsten lamp. For the HS ( $g=4$ )  $S_2$  state, the 140 K illumination, samples were continuously illuminated for 10 min using a 400 W tungsten lamp with filters to allow only near-infrared (NIR) light to reach the sample while the temperature was maintained with a continuous stream of liquid nitrogen-cooled nitrogen gas. We confirmed the presence of the HS ( $g=4$ ) and LS ( $g=2$ )  $S_2$  state by measuring the EPR spectra (Fig. 2A). From the XANES and XES spectra of the LS  $S_2$  and HS  $S_2$  states, we observe that HS  $S_2$  appears slightly reduced

compared to the LS form, suggesting that the effective charge density of the HS form may be lower than that of LS (Fig. 2B). As formal oxidation state and number of unpaired spins should be the same between the HS and LS S<sub>2</sub> state (although the total spin number differs, 1/2 or 5/2, due to exchange coupling of the four Mn), we speculated that different protonation states of the oxygen ligands or changes in geometry of the cluster in these two states shifts the effective charge density on Mn. The extended X-ray absorption fine structure (EXAFS) of the LS S<sub>2</sub> and HS S<sub>2</sub> states suggests that their structures are different from each other. The EXAFS data for the LS S<sub>2</sub> state fit well with the proposed right open structure with three short Mn-Mn interactions around 2.7–2.8 Å and one long Mn-Mn interaction around 3.3 Å. Meanwhile, the HS S<sub>2</sub> state fit well with two short Mn-Mn interactions around 2.7–2.8 Å and two long Mn-Mn interactions around 3.1–3.3 Å. These Mn-Mn interactions of the HS S<sub>2</sub> state do not match well with the closed cubane structure (left open) proposed by theoretical studies, where the numbers of short and long Mn-Mn interactions and Mn-Ca interactions remain the same in the HS S<sub>2</sub> and the LS S<sub>2</sub> states. We further showed that when we anneal the HS ( $g = 4$ ) S<sub>2</sub> state to 200 K in the dark, the EPR spectrum of the S<sub>2</sub>-g4 form converts back to the S<sub>2</sub>-g2 form (Fig. 2D). The EXAFS of the annealed S<sub>2</sub>-g4 form also goes back to the S<sub>2</sub>-g2 form, confirming the observation made using EPR spectroscopy. This implies a certain flexibility of the OEC in its geometric and electronic structure, although one state may be more preferable than the other under a given condition. Whether the HS S<sub>2</sub> state serves as an intermediate state between the LS S<sub>2</sub> and the S<sub>3</sub> state as proposed from theoretical modeling remains a question that we wish to answer from high-resolution crystal structures of these intermediate states at room temperature. Although the S<sub>2</sub> to S<sub>3</sub> transition is accompanied by structural changes of the cluster, the current data indicates that the closed-cubane-like structure may not be an intermediate that appears during this transition (see next section; Kern et al. 2018).

### **Room temperature crystal structure of the S<sub>2</sub> state from *T. elongatus***

Our improved crystallography datasets (Kern et al. 2018) allow us to examine the chemical structures of the catalytic center in each S-state, and in time-intervals between the S-state transitions. During the crystallography data acquisition, the S-state advancement was also confirmed by K $\beta_{1,3}$  XES collected simultaneously with the diffraction data, which serves as a diagnostic tool for the oxidation state of the OEC. This combined XES/XRD approach thus allows connecting the oxidation state

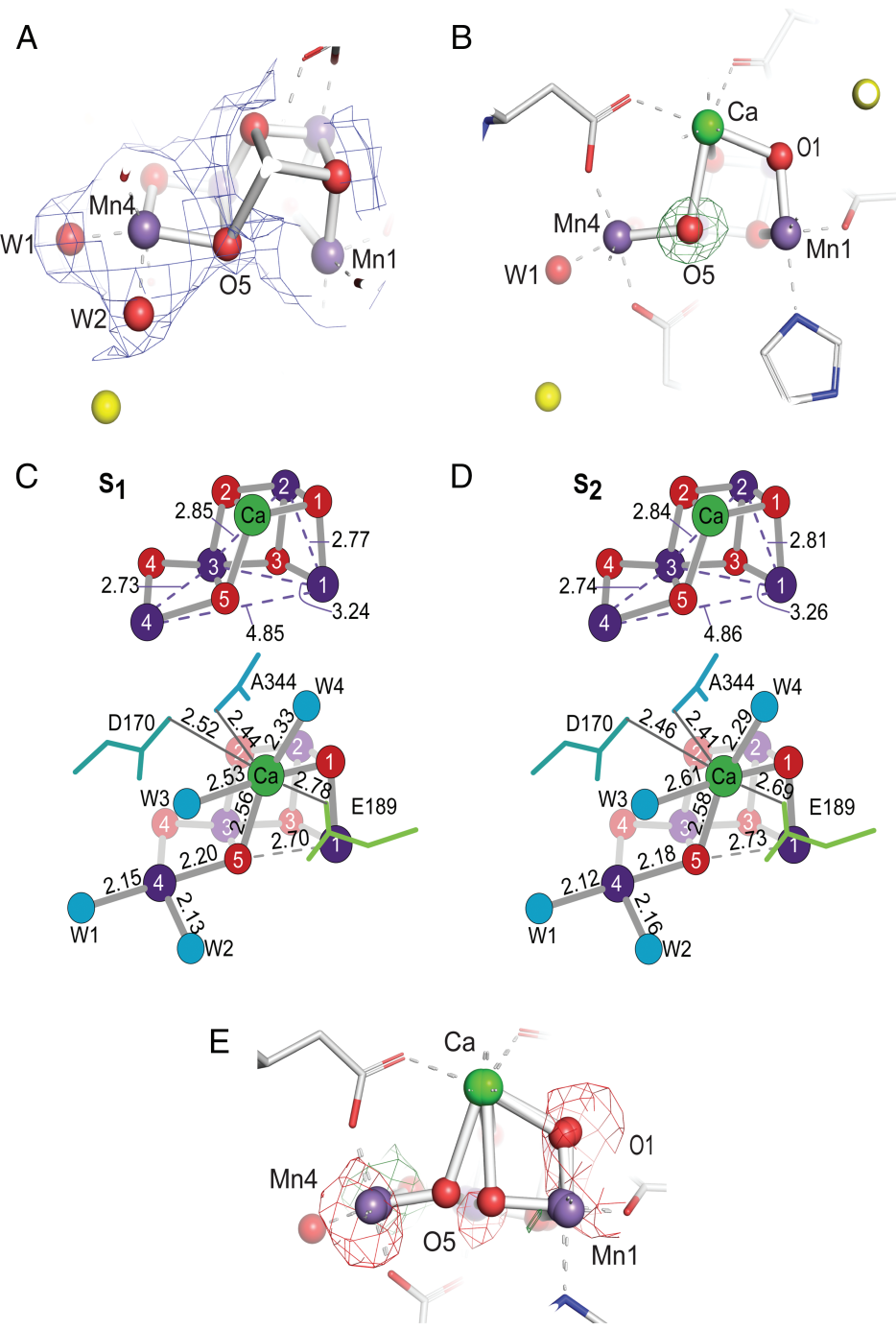
changes of Mn to the light-induced structural changes of the OEC and the protein. Based on the estimation from XES (in situ) as well as MIMS (ex situ, room temp.) and EPR (ex situ, cryo) we can conclude that the S<sub>1</sub> and S<sub>2</sub> states are the predominant species (>90%) in our dark (0F) and 1F data, respectively. Fig. 3A shows the 2mFo-DFc electron density and the model of the S<sub>2</sub> (1F) state. Bridging oxygens and terminal water positions can be clearly located in the Mn<sub>4</sub>CaO<sub>5</sub> cluster of the OEC with the current resolution of 2.08 Å. The geometry of three 2.7–2.8 Å and one 3.2–3.3 Å Mn-Mn distances is fundamentally the same as that in the dark S<sub>1</sub> state, which is also expected from the similarity of the S<sub>1</sub> and S<sub>2</sub> state EXAFS studies (Glöckner et al. 2013), with a right-open cubane Mn<sub>3</sub>CaO<sub>4</sub> moiety plus a di- $\mu$ -oxo bridged fourth Mn.

Upon S<sub>1</sub> to S<sub>2</sub> transition, a charge separation occurs at P<sub>680</sub> and an electron is transferred to the Q<sub>B</sub> site and one Mn is oxidized from +3 to +4. It has been widely accepted that the formal oxidation state of Mn in the S<sub>1</sub> and the S<sub>2</sub> state is Mn<sub>4</sub> (III<sub>2</sub>, IV<sub>2</sub>) and Mn<sub>4</sub> (III, IV<sub>3</sub>), respectively, based on the EPR exchange coupling scheme and supported by theory (Kulik et al. 2007, Krewald et al. 2015). The Mn<sub>4</sub>CaO<sub>5</sub> cluster in the S<sub>2</sub> state shows a clear right-open structure, in which there is no bond between Mn1 and O5. The Mn4-O5 distance is ~2.2 Å, while Mn1-O5 is ~2.70 Å in S<sub>1</sub> and 2.73 Å in S<sub>2</sub> (Fig. 3C,D). The trend in distance changes (albeit within the coordinate errors), suggests an increased asymmetry of the Mn4-O5-Mn1 positions and a shortening of Mn4-W1 when going from the S<sub>1</sub> to the S<sub>2</sub> state. This is consistent with Mn4 being oxidized at this stage, matching well with the formation of the S<sub>2</sub> state with the total spin ( $S_{\text{total}}$ ) of 1/2. However, this needs to await further confirmation by higher resolution data. The possibility that a small fraction of the HS S<sub>2</sub> state with a closed-cubane structure is also present is discussed in the next section.

### **Implication of the isomorphism and heterogeneity in the S<sub>2</sub> state**

As discussed above, there are many indications for the presence of two forms of the S<sub>2</sub> state (high-spin  $S_{\text{total}} = 5/2$  and low spin  $S_{\text{total}} = 1/2$  states, Fig. 1A) at least at cryogenic temperatures (Boussac et al. 1998a, 2018, Pantazis et al. 2012, Bovi et al. 2013, Cox et al. 2013, Isobe et al. 2014, Chatterjee et al. 2016). Nevertheless, the right-open S<sub>2</sub> state seems to be the one that best explains the diffraction data obtained at room temperature (Fig. 3A,C). To investigate if our data are also compatible with the presence of a different structural model for the S<sub>2</sub> state, we focused on the position of the O5

**Fig. 3.** Comparison of the MnCaO<sub>5</sub> cluster of the OEC between the S<sub>1</sub> and S<sub>2</sub> states. (A) 2mF<sub>o</sub>-DF<sub>c</sub> density (blue mesh) of the OEC in the S<sub>2</sub> state shown at 0.7σ contour level. In addition, the mF<sub>o</sub>-DF<sub>c</sub> difference density between the data and the model was plotted at 3.0σ contour level but no peaks are visible as the differences have low intensity, indicating a good fit of the model to the experimental data (B) O5 omit map density shown of the OEC in the S<sub>2</sub> state, contoured at 3.0σ (green mesh). (C) and (D) Atomic distances in the OEC averaged across both monomers in S<sub>1</sub> and S<sub>2</sub> states, respectively. Ca remains 8-coordinate upon insertion of Ox by way of movement of D1-Glu189 away from the OEC. (E) mF<sub>o</sub>-DF<sub>c</sub> difference density between the data and the model shown at +3.0σ (green) and -3.0σ (red) contour. This density was calculated using the 1:1 mixture of the open cubane (right open) and closed cubane (left open) models (Fig. 1B). The figure is adapted from Kern et al. (2018).



atom, which would undergo the largest structural change between the two proposed S<sub>2</sub> state models. In addition, an elongation of the Mn3-Mn4 or the shortening of the Mn1-Mn3 distances are expected according to the theoretical models for the two S<sub>2</sub> states. Fig. 3B shows the F<sub>obs</sub>-F<sub>calc</sub> omit map in the region of the OEC obtained from the S<sub>2</sub> (1F) data and a model in which the O5 was omitted. A clear single positive density feature is visible

at the position that was modeled for the O5 atom, indicating that the data allow to locate only one oxygen position and that the modeled position matches well with the experimental data. As a control, we considered the 1:1 mixture of the open cubane (right-open) and closed cubane (left-open) models, in which the coordinates for the closed cubane model were taken from the reference, Pantazis et al. 2012, and F<sub>obs</sub>-F<sub>calc</sub> electron density maps

(the difference between the experimental data and the model) were calculated (Fig. 3E). Clear difference density features at several positions, including a negative feature at the position of oxygen 5 in the closed cubane model, indicated that the 1:1 mixture model is not a good fit to the data. This implies that the right-open structure is a suitable model for the  $S_2$  (1F) state data under our experimental condition. Although a slight increase of B-factors for Mn and bridging oxygens between the OF and 1F data in both monomers can be seen, this can be explained mostly by the difference in resolution/data quality between the two data sets (2.05 vs 2.08 Å), and no clear evidence is observed under our experimental conditions for increased disorder in the  $S_2$  (1F) state data (Kern et al. 2018).

Although we do not see any evidence for the presence of more than one  $S_2$  structure in the 1F data under our conditions, we cannot exclude the presence of minor concentrations (< 20%) and further studies will be required to elucidate if such forms exist as transient states between the  $S_2$  and  $S_3$  states as proposed by some theoretical studies, in relation to the water-insertion pathway (Pantazis et al. 2012, Bovi et al. 2013, Siegbahn 2013, Isobe et al. 2014, 2015, Narzi et al. 2014, Shoji et al. 2015, Retegan et al. 2016, Ugur et al. 2016). We have taken the first step into this direction, by collecting X-ray diffraction data for two time points during the  $S_2$ - $S_3$  transition (150 µs and 400 µs after the second flash; Kern et al. 2018). The electron densities obtained and the isomorphous difference maps indicated some motion of Mn1 and Mn4 at the earlier stage (150 µs after the second flash) with O5 still staying close to Mn4 (~2.2 Å). A clear insertion of an additional oxygen next to Mn1 was observed in the later time point (400 µs after the second flash). At this point, there is no evidence supporting the proposed role of a left-open HS  $S_2$  state during this transition.

### Changes in the water network

Upon the  $S_1$  to  $S_2$  transition, it is known that one electron is extracted from the OEC, but without the release of the proton into the bulk, thus building up a positive charge in the OEC (Dau and Haumann 2008, Cox and Messinger 2013, Klauss et al. 2015). The response to such changes may appear in the hydrogen-bonding network around the OEC, because a proton may be parked near the OEC without being released to the bulk, or the proton still stays at the  $Mn_4CaO_5$  cluster in the  $S_2$  state, but the extra charge at the cluster is compensated by a rearrangement of the surroundings. We have observed changes in two sites around the OEC, one is next to oxygen O1 at a cluster of 5 waters (W26–W30) and the other next to

oxygen O4 at the W20 region (Fig. 4; Kern et al. 2018). Waters of the former five membered water ring change positions upon every S-state transition. In contrast, the change of W20 is observed only in the  $S_1$  to  $S_2$  step. In the dark-adapted  $S_1$  state the electron density for W20 is visible with about 70% occupancy (Fig. 4A), but this electron density disappears between OF ( $S_1$ ) and 1F ( $S_2$ ) (Fig. 4B). This could mean that either water W20 in the  $S_2$  state disappears or is not observed due to high mobility. ‘Disappearance’ means that the water molecule (W20) does not show up in the original position but may have moved to a new position. Higher mobility, on the other hand, means that the water molecule is still present in the same location, but due to, for example, flexibility in its orientation, the position is not well-defined. As a consequence, its occupancy becomes very low and the water cannot be clearly observed. While these two phenomena are difficult to differentiate from the crystallographic data, we speculate that W20 is not observed due to the higher mobility. This is based on the observation that no additional water density shows up in the proximal region upon the disappearance of the W20 density. In the recent work by Suga et al. (2017), the disappearance of the same water (W665 in their nomenclature) was reported in the 2F-dark difference map. Our result shows that this change in the W20 density actually occurs during the  $S_1$  to  $S_2$  transition, and not during the  $S_2$  to  $S_3$  transition. The removal of a weakly bound W20 is accompanied by small changes of the water network around Mn4 and O4, including W19 (bound to O4) and W1 (bound to Mn4). The W20 density is already weak in the dark state in comparison to other waters, indicating its higher mobility or lower occupancy. It is likely that the overall changes observed above are a consequence of the oxidation of Mn4 from +3 to +4 in the  $S_1$  to  $S_2$  transition and the connected increase in charge of the cluster (Klauss et al. 2012, Sakamoto et al. 2017). Thus, we speculate that the structural changes observed in the W20 region are a consequence of charge compensation around the OEC. Interestingly, the W20 water density becomes visible again in the 3F ( $S_0$ ) data, implying that its hydrogen-bonding network comes back upon the  $S_3$  to  $S_0$  transition.

### Summary

In this review, we examined the room temperature crystal structure to investigate the presence/absence of the structural isomers in the  $S_2$  state, in comparison to other spectroscopic studies that include X-ray absorption spectroscopy and EPR, and theoretical calculations. In our crystallography experiment under catalytically functional conditions (at room temperature, pH 6.5), the

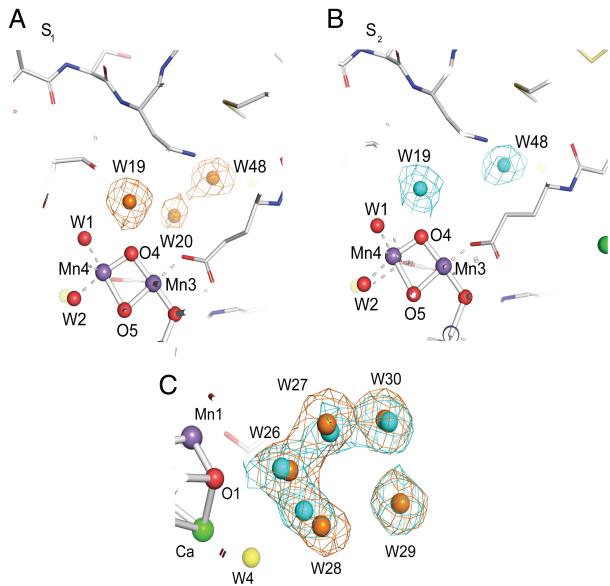


**Fig. 4.** Comparison of the water environment of the OEC between the  $S_1$  and  $S_2$  states. (A and B) Water environment of the OEC at the O4 water chain (A and B) and next to O1(C) in the  $S_1$  (OF, brown) and  $S_2$  (1F, blue) states. We note that water 20 is highly unstable in position and there is not sufficient density in the  $S_2$  state data to model the water 20 position. (C) The overlaid  $2mF_o - DF_c$  density maps at  $1.5\sigma$  contour level of the  $S_1$  (OF, brown) and  $S_2$  (1F, blue) states show the changes in water positions. The O1-W26 distance changes from 3.09 to 3.01 Å upon transition from  $S_1$  to  $S_2$ . The figures are adapted from Kern et al. (2018).

dominant form of the  $Mn_4CaO_5$  cluster in the  $S_2$  state is the right-open structure that is similar to the low spin configuration ( $S_{\text{total}} = 1/2$ ) form from the EXAFS result. We did not observe the closed-cubane form of the cluster (left-open) of the  $S_2$  state at this pH. The X-ray diffraction data collected at the intermediate time points (150 and 400 µs) during the  $S_2$ - $S_3$  transition, albeit at limited resolution, also did not provide any indication for the presence of a left-open (closed cubane) form of the OEC. Thus, the results suggest that the presence/appearance of the high-spin, closed cubane form may not be necessary for the  $S_2$  to  $S_3$  transition under catalytic conditions. On the other hand, the low-spin and the high-spin form of the  $S_2$  state do appear under other experimental conditions as evidenced by the series of EPR studies, and our EXAFS studies under cryogenic temperature have shown that the OEC structures of these two forms differ in its Mn-Mn distances. However, the structure of this high-spin form may not be exactly the same as the closed cubane form proposed so far, as the current EXAFS result does not match with the metal–metal distances expected in the closed cubane motif. Thus, high-resolution crystal structures for several time points during the  $S_2$ - $S_3$  transition together with structures under

different conditions (e.g. higher pH) will be necessary to understand the actual structure of the high-spin form, and to bridge between the catalytic mechanism and the structural parameters.

## Author contributions

R.C., M.H.C., J.M., V.K.Y., J.K. and J.Y. wrote the paper with contributions from L.L., S.G., F.D.F., I.D.Y., M.I., C. d.-L. and A.Z.

**Acknowledgements** – This work was supported by the NIH Grants GM110501 (J.Y.), GM126289 (J.K.) and GM055302 (V.K.Y.), the Director, Office of Science, Office of Basic Energy Sciences (OBES), Division of Chemical Sciences, Geosciences, and Biosciences of the Department of Energy (DOE) (J.Y., V.K.Y.), the Artificial Leaf Project (K&A Wallenberg Foundation 2011.0055) and Vetenskapsrådet (2016-05183) (J.M.), and the Ruth L. Kirschstein National Research Service Award (GM116423-02, F.D.F.). Use of the LCLS, SLAC National Accelerator Laboratory, is supported by the U.S. DOE, Office of Science, OBES under Contract No. DE-AC02-76SF00515. We thank the Deutsche Forschungsgemeinschaft (DFG) for financial support to the collaborative research center on Protonation Dynamics in Protein Function (SFB 1078, project A5 Zouni/Dobbek [M.I., A.Z.]).

## References

- Beck WF, Brudvig GW (1986) Binding of amines to the O2-evolving center of photosystem-II. Biochemistry 25: 6479–6486
- Boussac A, Rutherford AW (1988) Nature of the inhibition of the oxygen-evolving enzyme of photosystem II induced by NaCl washing and reversed by the addition of  $Ca^{2+}$  or  $Sr^{2+}$ . Biochemistry 27: 3476–3483
- Boussac A, Girerd J-J, Rutherford AW (1996) Conversion of the spin state of the manganese complex in photosystem II induced by near-infrared light. Biochemistry 35: 6984–6989
- Boussac A, Un S, Horner O, Rutherford AW (1998a) High-spin states ( $S \geq 5/2$ ) of the photosystem II manganese complex. Biochemistry 37: 4001–4007
- Boussac A, Kuhl H, Un S, Rögner M, Rutherford AW (1998b) Effect of near-infrared light on the  $S_2$ -state of the manganese complex of photosystem II from *Synechococcus elongatus*. Biochemistry 37: 8995–9000
- Boussac A, Sugiura M, Rutherford AW, Dorlet P (2009) Complete EPR spectrum of the S-3-state of the oxygen-evolving photosystem II. J Am Chem Soc 131: 5050–5051
- Boussac A, Rutherford AW, Sugiura M (2015) Electron transfer pathways from the  $S_2$ -states to the  $S_3$ -states

- either after a Ca<sup>2+</sup>/Sr<sup>2+</sup> or a Cl<sup>-</sup>/I<sup>-</sup> exchange in photosystem II from. *Biochim Biophys Acta* 1847: 576–586
- Boussac A, Ugur I, Marion A, Sugiura M, Kaila VRI, Rutherford AW (2018) The low spin - high spin equilibrium in the S<sub>2</sub>-state of the water oxidizing enzyme. *Biochim Biophys Acta* 1859: 342–356
- Bovi D, Narzi D, Guidoni L (2013) The S<sub>2</sub> state of the oxygen-evolving complex of photosystem II explored by QM/MM dynamics: spin surfaces and metastable states suggest a reaction path towards the S<sub>3</sub> state. *Angew Chem Int Edit* 52: 11744–11749
- Brudvig GW, Casey JL, Sauer K (1983) The effect of temperature on the formation and decay of the multiline EPR signal species associated with photosynthetic oxygen evolution. *Biochim Biophys Acta* 723: 366–371
- Casey JL, Sauer K (1984) EPR detection of a cryogenically photogenerated intermediate in photosynthetic oxygen evolution. *Biochim Biophys Acta* 767: 21–28
- Charlot M-F, Boussac A, Blondin G (2005) Towards a spin coupling model for the Mn<sub>4</sub> cluster in photosystem II. *Biochim Biophys Acta* 1708: 120–132
- Chatterjee R, Han G, Kern J, Gul S, Fuller FD, Garachchenko A, Young ID, Weng TC, Nordlund D, Alonso-Mori R, Bergmann U, Sokaras D, Hatakeyama M, Yachandra VK, Yano J (2016) Structural changes correlated with magnetic spin state isomorphism in the S<sub>2</sub> state of the Mn<sub>4</sub>CaO<sub>5</sub> cluster in the oxygen-evolving complex of photosystem II. *Chem Sci* 7: 5236–5248
- Cox N, Messinger J (2013) Reflections on substrate water and dioxygen formation. *Biochim Biophys Acta* 1827: 1020–1030
- Cox N, Rapatskiy L, Su JH, Pantazis DA, Sugiura M, Kulik L, Dorlet P, Rutherford AW, Neese F, Boussac A, Lubitz W, Messinger J (2011) Effect of Ca<sup>2+</sup>/Sr<sup>2+</sup> substitution on the electronic structure of the oxygen-evolving complex of photosystem II: a combined multifrequency EPR, <sup>55</sup>Mn-ENDOR, and DFT study of the S<sub>2</sub> state. *J Am Chem Soc* 133: 3635–3648
- Cox N, Pantazis DA, Neese F, Lubitz W (2013) Biological water oxidation. *Acc Chem Res* 46: 1588–1596
- Cox N, Retegan M, Neese F, Pantazis DA, Boussac A, Lubitz W (2014) Electronic structure of the oxygen evolving complex in photosystem II prior to O-O bond formation. *Science* 345: 804–808
- Dau H, Haumann M (2008) The manganese complex of photosystem II in its reaction cycle – basic framework and possible realization at the atomic level. *Coord Chem Rev* 252: 273–295
- Debus RJ (1992) The manganese and calcium-ions of photosynthetic oxygen evolution. *Biochim Biophys Acta* 1102: 269–352
- Debus RJ (2008) Protein ligation of the photosynthetic oxygen-evolving center. *Coord Chem Rev* 252: 244–258
- Dismukes GC, Siderer Y (1981) Intermediates of a polynuclear manganese cluster involved in photosynthetic oxidation of water. *Proc Natl Acad Sci USA* 78: 274–278
- Fransson T, Chatterjee R, Fuller FD, Gul S, Weninger C, Sokaras D, Kroll T, Alonso-Mori R, Bergmann U, Kern J, Yachandra VK, Yano J (2018) X-ray emission spectroscopy as an in situ diagnostic tool for X-ray crystallography of metalloproteins using an X-ray free-electron laser. *Biochemistry* 57: 4629–4637
- Fuller FD, Gul S, Chatterjee R, Burgie ES, Young ID, Lebrette H, Srinivas V, Brewster AS, Michels-Clark T, Clinger JA, Andi B, Ibrahim M, Pastor E, de Lichtenberg C, Hussein R, Pollock CJ, Zhang M, Stan CA, Kroll T, Fransson T, Weninger C, Kubin M, Aller P, Lassalle L, Brauer P, Miller MD, Amin M, Koroidov S, Roessler CG, Allaire M, Sierra RG, Docker PT, Glowina JM, Nelson S, Koglin JE, Zhu DL, Chollet M, Song S, Lemke H, Liang MN, Sokaras D, Alonso-Mori R, Zouni A, Messinger J, Bergmann U, Boal AK, Bollinger JM, Krebs C, Hogbom M, Phillips GN, Vierstra RD, Sauter NK, Orville AM, Kern J, Yachandra VK, Yano J (2017) Drop-on-demand sample delivery for studying biocatalysts in action at X-ray free-electron lasers. *Nat Methods* 14: 443–449
- Glatzel P, Bergmann U, Yano J, Visser H, Robblee JH, Gu W, de Groot FMF, Christou G, Pecoraro VL, Cramer SP, Yachandra VK (2004) The electronic structure of Mn in oxides, coordination complexes, and the oxygen-evolving complex of photosystem II studied by resonant inelastic X-ray scattering. *J Am Chem Soc* 126: 9946–9959
- Glatzel P, Schroeder H, Pushkar Y, Boron T III, Mukherjee S, Christou G, Pecoraro VL, Messinger J, Yachandra VK, Bergmann U, Yano J (2013) Electronic structural changes of Mn in the oxygen-evolving complex of photosystem II during the catalytic cycle. *Inorg Chem* 52: 5642
- Glöckner C, Kern J, Broser M, Zouni A, Yachandra V, Yano J (2013) Structural changes of the oxygen-evolving complex in photosystem II during the catalytic cycle. *J Biol Chem* 288: 22607–22620
- Guiles RD, Zimmermann JL, McDermott AE, Yachandra VK, Cole JL, Dexheimer SL, Britt RD, Wieghardt K, Bossek U, Sauer K, Klein MP (1990) The S<sub>3</sub> state of photosystem II: differences between the structure of the manganese complex in the S<sub>2</sub> and S<sub>3</sub> states determined by X-ray absorption spectroscopy. *Biochemistry* 29: 471–485
- Haddy A (2007) EPR spectroscopy of the manganese cluster of photosystem II. *Photosynth Res* 92: 357–368

- Haddy A, Lakshmi KV, Brudvig GW, Frank HA (2004) Q-band EPR of the S<sub>2</sub> state of photosystem II confirms an S = 5/2 origin of the X-band g = 4.1 signal. *Biophys J* 87: 2885–2896
- Hansson Ö, Andréasson L-E (1982) EPR-detectable magnetically interacting manganese ions in the photosynthetic oxygen-evolving system after continuous illumination. *Biochim Biophys Acta* 679: 261–268
- Hansson Ö, Aasa R, Vängard T (1987) The origin of the multiline and g = 4.1 electron-paramagnetic resonance signals from the oxygen-evolving system of photosystem II. *Biophys J* 51: 825–832
- Haumann M, Müller C, Liebisch P, Iuzzolino L, Dittmer J, Grabolle M, Neisius T, Meyer-Klaucke W, Dau H (2005) Structural and oxidation state changes of the photosystem II manganese complex in four transitions of the water oxidation cycle (S<sub>0</sub> → S<sub>1</sub>, S<sub>1</sub> → S<sub>2</sub>, S<sub>2</sub> → S<sub>3</sub>, and S<sub>3</sub>, S<sub>4</sub> → S<sub>0</sub>) characterized by X-ray absorption spectroscopy at 20 K and room temperature. *Biochemistry* 44: 1894–1908
- Isobe H, Shoji M, Yamanaka S, Mino H, Umena Y, Kawakami K, Kamiya N, Shen JR, Yamaguchi K (2014) Generalized approximate spin projection calculations of effective exchange integrals of the CaMn<sub>4</sub>O<sub>5</sub> cluster in the S-1 and S-3 states of the oxygen evolving complex of photosystem II. *Phys Chem Chem Phys* 16: 11911–11923
- Isobe H, Shoji M, Shen JR, Yamaguchi K (2015) Strong coupling between the hydrogen bonding environment and redox chemistry during the S<sub>2</sub> to S<sub>3</sub> transition in the oxygen-evolving complex of photosystem II. *J Phys Chem B* 119: 13922–13933
- Isobe H, Shoji M, Shen JR, Yamaguchi K (2016) Chemical equilibrium models for the S-3 state of the oxygen-evolving complex of photosystem II. *Inorg Chem* 55: 502–511
- Kern J, Alonso-Mori R, Tran R, Hattne J, Gildea RJ, Echols N, Glöckner C, Hellmich J, Laksmono H, Sierra RG, Lassalle-Kaiser B, Koroidov S, Lampe A, Han GY, Gul S, DiFiore D, Milathianaki D, Fry AR, Miahnahri A, Schafer DW, Messerschmidt M, Seibert MM, Koglin JE, Sokaras D, Weng TC, Sellberg J, Latimer MJ, Grosse-Kunstleve RW, Zwart PH, White WE, Glatzel P, Adams PD, Bogan MJ, Williams GJ, Boutet S, Messinger J, Zouni A, Sauter NK, Yachandra VK, Bergmann U, Yano J (2013) Simultaneous femtosecond X-ray spectroscopy and diffraction of photosystem II at room temperature. *Science* 340: 491–495
- Kern J, Tran R, Alonso-Mori R, Koroidov S, Echols N, Hattne J, Ibrahim M, Gul S, Laksmono H, Sierra RG, Gildea RJ, Han G, Hellmich J, Lassalle-Kaiser B, Chatterjee R, Brewster AS, Stan CA, Glöckner C, Lampe A, DiFiore D, Milathianaki D, Fry AR, Seibert MM, Koglin JE, Gallo E, Uhlig J, Sokaras D, Weng TC, Zwart PH, Skinner DE, Bogan MJ, Messerschmidt M, Glatzel P, Williams GJ, Boutet S, Adams PD, Zouni A, Messinger J, Sauter NK, Bergmann U, Yano J, Yachandra VK (2014) Taking snapshots of photosynthetic water oxidation using femtosecond X-ray diffraction and spectroscopy. *Nature Comm* 5: 4371
- Kern J, Chatterjee R, Young ID, Fuller FD, Lassalle L, Ibrahim M, Gul S, Fransson T, Brewster AS, Alonso-Mori R, Hussein R, Zhang M, Douthit L, de Lichtenberg C, Cheah MH, Shevela D, Wersig J, Seufert I, Sokaras D, Pastor E, Weninger C, Kroll T, Sierra RG, Aller P, Butryn A, Orville AM, Liang M, Batyuk A, Koglin JE, Carbojo S, Boutet S, Moriarty NW, Holton JM, Dobbek H, Adams PD, Bergmann U, Sauter NK, Zouni A, Messinger J, Yano J, Yachandra VK (2018) Structures of the intermediates of Kok's photosynthetic water oxidation clock. *Nature* 563: 421–425
- Kim CJ, Bao H, Burnap RL, Debus RJ (2018) Impact of D1-V185 on the water molecules that facilitate O<sub>2</sub> formation by the catalytic Mn<sub>4</sub>CaO<sub>5</sub> cluster in photosystem II. *Biochemistry* 57: 4299–4311
- Klauss A, Haumann M, Dau H (2012) Alternating electron and proton transfer steps in photosynthetic water oxidation. *Proc Natl Acad Sci USA* 109: 16035–16040
- Klauss A, Haumann M, Dau H (2015) Seven steps of alternating electron and proton transfer in photosystem II water oxidation traced by time-resolved photothermal beam deflection at improved sensitivity. *J Phys Chem B* 119: 2677–2689
- Kok B, Forbush B, McGloin M (1970) Cooperation of charges in photosynthetic oxygen evolution. A linear four step mechanism. *Photochem Photobiol* 11: 457–475
- Krewald V, Retegan M, Cox N, Messinger J, Lubitz W, DeBeer S, Neese F, Pantazis DA (2015) Metal oxidation states in biological water splitting. *Chem Sci* 6: 1676–1695
- Krewald V, Retegan M, Neese F, Lubitz W, Pantazis DA, Cox N (2016) Spin state as a marker for the structural evolution of nature's water splitting catalyst. *Inorg Chem* 55: 488–501
- Kulik LV, Epel B, Lubitz W, Messinger J (2007) Electronic structure of the Mn<sub>4</sub>OxCa cluster in the S-0 and S-2 states of the oxygen-evolving complex of photosystem II based on pulse Mn-55-ENDOR and EPR spectroscopy. *J Am Chem Soc* 129: 13421–13435
- Liang WC, Latimer MJ, Dau H, Roelofs TA, Yachandra VK, Sauer K, Klein MP (1994) Correlation between structure and magnetic spin state of the manganese cluster in the oxygen-evolving complex of photosystem II in the S<sub>2</sub> state: determination by X-ray absorption spectroscopy. *Biochemistry* 33: 4923–4932
- Lubitz W, Cox N, Rapatskiy L, Lohmiller T, Navarro MP, Ames W, Pantazis D, Neese F, Boussac N, Messinger J (2014) Light-induced water oxidation in photosynthesis. *J Biol Inorg Chem* 19: S350–S350

- Nakamura S, Ota K, Shibuya Y, Noguchi T (2016) Role of a water network around the Mn<sub>4</sub>CaO<sub>5</sub> cluster in photosynthetic water oxidation: a Fourier transform infrared spectroscopy and quantum mechanics/molecular mechanics calculation study. *Biochemistry* 55: 597–607
- Narzi D, Bovi D, Guidoni L (2014) Pathway for Mn-cluster oxidation by tyrosine-Z in the S-2 state of photosystem II. *Proc Natl Acad Sci USA* 111: 8723–8728
- Noguchi T (2008) FTIR detection of water reactions in the oxygen-evolving center of photosystem II. *Philos Trans R Soc Lond B Biol Sci* 363: 1189–1194
- Noguchi T (2015) Fourier transform infrared difference and time-resolved infrared detection of the electron and proton transfer dynamics in photosynthetic water oxidation. *Biochim Biophys Acta* 1847: 35–45
- Pantazis DA, Ames W, Cox N, Lubitz W, Neese F (2012) Two interconvertible structures that explain the spectroscopic properties of the oxygen-evolving complex of photosystem II in the S<sub>2</sub> state. *Angew Chem Int Edit* 51: 9935–9940
- de Paula JC, Brudvig GW (1985) Magnetic properties of manganese in the photosynthetic oxygen-evolving complex. *J Am Chem Soc* 107: 2643–2648
- Peloquin JM, Britt RD (2001) EPR/ENDOR characterization of the physical and electronic structure of the OEC Mn cluster. *Biochim Biophys Acta* 1503: 96–111
- Peloquin JM, Campbell KA, Randall DW, Evanchik MA, Pecoraro VL, Armstrong WH, Britt RD (2000) 55Mn ENDOR of the S2-state multiline EPR signal of photosystem II: implications on the structure of the tetranuclear cluster. *J Am Chem Soc* 122: 10926–10942
- Pokhrel R, Brudvig GW (2014) Oxygen-evolving complex of photosystem II: correlating structure with spectroscopy. *Phys Chem Chem Phys* 16: 11812–11821
- Pushkar Y, Yano J, Sauer K, Boussac A, Yachandra VK (2008) Structural changes in the Mn<sub>4</sub>Ca cluster and the mechanism of photosynthetic water splitting. *Proc Natl Acad Sci USA* 105: 1879–1884
- Randall DW, Sturgeon BE, Ball JA, Lorigan GA, Chan MK, Klein MP, Armstrong WH, Britt RD (1995) 55Mn ESE-ENDOR of a mixed valence Mn(III)Mn(IV) complex: comparison with the Mn cluster of the photosynthetic oxygen-evolving complex. *J Am Chem Soc* 117: 11780–11789
- Renger G (2008) Functional pattern of photosystem II. In: Primary Processes of Photosynthesis. RSC Publishing, Cambridge, UK, pp 237–290
- Renger G (2012) Mechanism of light induced water splitting in photosystem II of oxygen evolving photosynthetic organisms. *Biochim Biophys Acta* 1817: 1164–1176
- Retegan M, Cox N, Lubitz W, Neese F, Pantazis DA (2014) The first tyrosyl radical intermediate formed in the S-2-S-3 transition of photosystem II. *Phys Chem Chem Phys* 16: 11901–11910
- Retegan M, Krewald V, Mamedov F, Neese F, Lubitz W, Cox N, Pantazis DA (2016) A five-coordinate Mn(IV) intermediate in biological water oxidation: spectroscopic signature and a pivot mechanism for water binding. *Chem Sci* 7: 72–84
- Sakamoto H, Shimizu T, Nagao R, Noguchi T (2017) Monitoring the reaction process during the S-2 → S-3 transition in photosynthetic water oxidation using time-resolved infrared spectroscopy. *J Am Chem Soc* 139: 2022–2029
- Shoji M, Isobe H, Yamaguchi K (2015) QM/MM study of the S-2 to S-3 transition reaction in the oxygen-evolving complex of photosystem II. *Chem Phys Lett* 636: 172–179
- Shoji M, Isobe H, Tanaka A, Fukushima Y, Kawakami K, Umena Y, Kamiya N, Nakajima T, Yamaguchi K (2018) Understanding two different structures in the dark stable state of the oxygen-evolving complex of photosystem II: applicability of the jahn–teller deformation formula. *Chem Photo Chem* 2: 257–270
- Siegbahn PEM (2013) Water oxidation mechanism in photosystem II, including oxidations, proton release pathways, O-O bond formation and O-2 release. *Biochim Biophys Acta* 1827: 1003–1019
- Suga M, Akita F, Sugahara M, Kubo M, Nakajima Y, Nakane T, Yamashita K, Umena Y, Nakabayashi M, Yamane T, Nakano T, Suzuki M, Masuda T, Inoue S, Kimura T, Nomura T, Yonekura S, Yu LJ, Sakamoto T, Motomura T, Chen JH, Kato Y, Noguchi T, Tono K, Joti Y, Kameshima T, Hatsui T, Nango E, Tanaka R, Naitow H, Matsura Y, Yamashita A, Yamamoto M, Nureki O, Yabashi M, Ishikawa T, Iwata S, Shen JR (2017) Light-induced structural changes and the site of O=O bond formation in PSII caught by XFEL. *Nature* 543: 131–135
- Ugur I, Rutherford AW, Kaila VRI (2016) Redox-coupled substrate water reorganization in the active site of photosystem II—the role of calcium in substrate water delivery. *Biochim Biophys Acta* 1857: 740–748
- Umena Y, Kawakami K, Shen J-R, Kamiya N (2011) Crystal structure of oxygen-evolving photosystem II at a resolution of 1.9 angstrom. *Nature* 473: 55–60
- Wydrzynski T, Satoh S (eds) (2005) Photosystem II: The Light-Driven Water:Plastoquinone Oxidoreductase. Springer, Dordrecht
- Yamaguchi K, Shoji M, Isobe H, Yamanaka S, Umena Y, Kawakami K, Kamiya N (2017) On the guiding principles for understanding of geometrical structures of the CaMn<sub>4</sub>O<sub>5</sub> cluster in oxygen-evolving complex of photosystem II. Proposal of estimation formula of structural deformations via the Jahn-teller effects. *Mol Phys* 115: 636–666

- Yano J, Yachandra VK (2014) Mn<sub>4</sub>Ca cluster in photosynthesis: where and how water is oxidized to dioxygen. *Chem Rev* 114: 4175–4205
- Young ID, Ibrahim M, Chatterjee R, Gul S, Fuller FD, Koroidov S, Brewster AS, Tran R, Alonso-Mori R, Kroll T, Michels-Clark T, Laksmono H, Sierra RG, Stan CA, Hussein R, Zhang M, Douthit L, Kubin M, de Lichtenberg C, Pham LV, Nilsson H, Cheah MH, Shevela D, Saracini C, Bean MA, Seuffert I, Sokaras D, Weng TC, Pastor E, Weninger C, Fransson T, Lassalle L, Brauer P, Aller P, Docker PT, Andi B, Orville AM, Glownia JM, Nelson S, Sikorski M, Zhu DL, Hunter MS, Lane TJ, Aquila A, Koglin JE, Robinson J, Liang MN, Boutet S, Lyubimov AY, Uervirojnakorn M, Moriarty NW, Liebschner D, Afonine PV, Waterman DG, Evans G, Wernet P, Dobbek H, Weis WI, Brunger AT, Zwart PH, Adams PD, Zouni A, Messinger J, Bergmann U, Sauter NK, Kern J, Yachandra VK, Yano J (2016) Structure of photosystem II and substrate binding at room temperature. *Nature* 540: 453–457
- Zimmermann JL, Rutherford AW (1984) Electron-paramagnetic-res studies of the oxygen-evolving enzyme of photosystem-II. *Biochim Biophys Acta* 767: 160–167
- Zimmermann JL, Rutherford AW (1986) Electron-paramagnetic resonance properties of the S-2 state of the oxygen-evolving complex of photosystem-II. *Biochemistry* 25: 4609–4615